Transverse Alignment of Fibers in a Periodically Sheared Suspension: An Absorbing Phase Transition with a Slowly Varying Control Parameter

Alexandre Franceschini,[1] Emmanouela Filippidi,[1] Elisabeth Guazzelli,[2] and David J. Pine[1]

[1]*Center for Soft Matter Research, Department of Physics, New York University, 4 Washington Place, New York, New York 10003, USA*
[2]*IUSTI-CNRS UMR 6595–Polytech Marseille – Aix-Marseille Université, 5 rue Enrico Fermi, 13453 Marseille Cedex 13, France*

(Received 28 July 2011; published 16 December 2011)

Shearing solutions of fibers or polymers tends to align fiber or polymers in the flow direction. Here, non-Brownian rods subjected to oscillatory shear align perpendicular to the flow while the system undergoes a nonequilibrium absorbing phase transition. The slow alignment of the fibers can drive the system through the critical point and thus promote the transition to an absorbing state. This picture is confirmed by a universal scaling relation that collapses the data with critical exponents that are consistent with conserved directed percolation.

DOI: 10.1103/PhysRevLett.107.250603 PACS numbers: 64.70.km, 05.65.+b, 05.70.Ln, 83.10.Pp

When a fiber suspension is subjected to steady shear flow, the fibers generally align in the flow direction [1,2]. This alignment of fibers is most dramatic for semidilute and more concentrated suspensions of stiff fibers, but occurs for flexible fibers as well [3], including polymer solutions and melts at moderate to high shear rates [4]. Controlling fiber alignment is important for the manufacture of paper, high-strength polymers, reinforced rubbers, and other materials [5,6]. Alignment, whether local or global, has been well documented in nematic liquid crystals [7], vibrated granular rods [8,9], and elongated colloids [10].

In this Letter, we show that when a suspension of neutrally buoyant non-Brownian fibers is subjected to oscillatory shear strain, the fibers can align perpendicular to the flow. This alignment occurs over a finite range of strain amplitudes and is governed by a subtle interplay between fiber orientation and short-range interactions through an athermal (nonequilibrium) process known as *random organization* [11,12]. At low strain amplitudes, we find that random organization, which proceeds through collision-induced fluctuations, occurs without significant alignment of fibers. By contrast, as the critical strain amplitude is increased, collision-induced fluctuations cause the fibers to align. In both cases, the system ultimately reaches a steady state in which fluctuations cease, provided the strain amplitude γ is below some critical value γ_c. For $\gamma > \gamma_c$, the system fluctuates about a steady state and the alignment of fibers is diminished. The transition between the nonfluctuating and fluctuating steady states belongs to a broad class of nonequilibrium phase transitions called *absorbing phase transitions* that have been linked to directed percolation [13–15]. The key (and unique) point here is that fiber orientation acts to produce a time-dependent control parameter that can drive the system through the critical point of an absorbing phase transition. This leads to unusual behavior in which the nonequilibrium critical phase transition of the system is delayed as the system hovers near criticality over a range of strain amplitudes.

Originally developed to understand sheared suspensions [11], random organization has also been used as a framework to understand periodically driven vortices in superconductors [16] and the phenomenon of plastic depinning [17]. The basic mechanism is most simply understood for a non-Brownian suspension of spheres. A suspension is subjected to periodic shearing, which initially causes nearby particles to collide. However, as periodic straining continues, these collisions drive the suspension towards a configuration in which all particles avoid each other. When they do, each particle simply retraces a reversible trajectory, returning to the same position after each cycle such that the periodically sampled configuration does not change with time. Above the threshold, a finite fraction of the objects continues to collide and fluctuate. By using fibers, we introduce orientational degrees of freedom in addition to the translational degrees of freedom present for the case of spheres. It is this additional degree of freedom that leads to a time-dependent control parameter and the unusual critical behavior it produces.

Our samples are nylon fibers of length $l = 1.52 \pm 0.14$ mm and diameter $d = 0.140 \pm 0.001$ mm ($l/d \approx 11$) dispersed in a Newtonian liquid of viscosity 1 Pa s. The liquid is an aqueous solution of triton X-100, a nonionic surfactant, and $ZnCl_2$ [18]. The concentrations are adjusted to match the fiber density and refractive index, thus avoiding sedimentation and rendering the suspension transparent. About 1% of the fibers are dyed with Rhodamine 6G so that their centers and orientations can be tracked. The fiber volume fraction c is varied from 0.05 to 0.20 in steps of 0.05, all above the overlap threshold $c^\star = \frac{3}{2}(d/l)^2 = 0.013$ and below the isotropic-to-nematic concentration $c_i = 3.34(d/l) = 0.32$ [10].

Suspensions are placed between concentric cylinders of a transparent Couette cell thermostated at 22 °C, as shown in Fig. 1. The inner cylinder, driven by a rheometer head, is rotated back and forth through an angle ψ to produce an oscillatory time-dependent strain $\gamma \sin\omega t$ with frequency

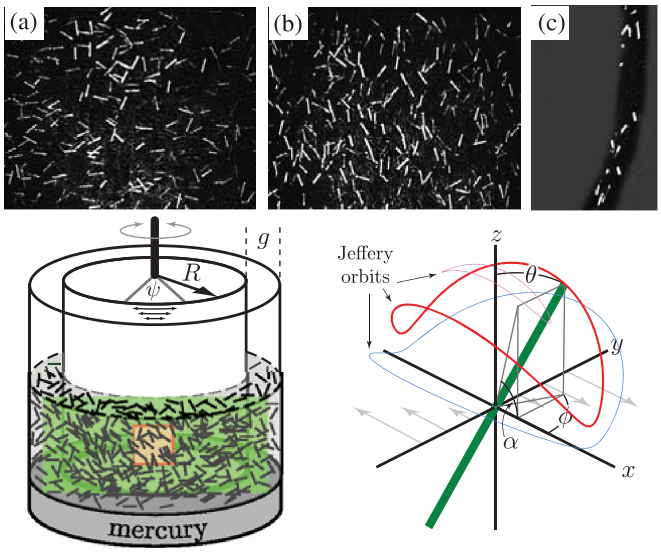

FIG. 1 (color). Upper row. Fluorescing fibers can be seen throughout the thickness of the gap: x-z images of the suspension (a) before and (b) after a run at $\gamma = 2.60$ with $c = 0.15$. (c) Top view of the gap. Bottom row. Left: Experimental setup: the shaded orange area shows the 1 cm^2 region that is imaged in the x-z plane. Right: x-y-z coordinate system, chosen to correspond to the flow, velocity gradient, and vorticity directions, respectively. Three Jeffery orbits are shown in different colors, with the corresponding rod shown in green only for the red orbit. The angles θ and ϕ are the polar and azimuthal angles, respectively, of the rod. The orientation of the fiber projected onto the x-z plane is α, as shown.

ω and strain amplitude $\gamma = \psi R/g$, where $R = 25$ mm is the radius of the inner cylinder and $g = 2.2$ mm the gap between cylinders.

Samples are sheared at a high oscillatory strain for 30 minutes ($\gamma = 10$, $\omega \approx 3$ rad s^{-1} and Reynolds number Re ≈ 0.15) to suppress sample history and ensure good mixing. After a 1 min rest, a measurement begins by subjecting the suspension to an oscillatory strain of amplitude γ and constant frequency, typically 0.04 Hz, while keeping $\mathrm{Re} = \omega\gamma g^2\rho/\eta \approx 10^{-3}$ to assure that inertial effects are unimportant.

A section of the Couette cell is illuminated with a sheet of green 532 nm laser light, which excites the dyed fibers. The central section of the illuminated volume is viewed with a digital camera, as shown in Fig. 1. Images, consisting of x-z projections of the dyed fibers, are recorded with a digital CCD camera once per cycle in synchronization with the oscillatory shear strain. By fitting the imaged particles with ellipses, their centers of mass and orientation are tracked through time [19].

Isolated fibers subjected to oscillatory shear flow at low Re trace out reversible trajectories [20], which are small sections ($\lesssim 5\%$) of their *Jeffery orbits* [21]. When viewed stroboscopically, fibers executing reversible trajectories appear as stationary objects with fixed positions and orientations. For a given cycle, we observe that some fraction of fibers execute reversible trajectories, while the remaining fraction collide with one another and thus are displaced from their previous positions and orientations. We refer to this irreversible motion as *activity*, and characterize it quantitatively by the active fraction f_a, consistent with terminology used for absorbing phase transitions [13–15]. The activity is quantitatively measured by the single-cycle translational and orientational mean square particle displacements. We measure the x-z projections of these quantities, which we write as $\langle \Delta r_1^2 \rangle$ and $\langle \Delta \alpha_1^2 \rangle$, respectively, and which are proportional to f_a.

As in previous reports [11,22], we find that the activity has a rheological signature. The complex viscosity $\eta^* = \eta' + i\eta''$ of a non-Brownian suspension in a Newtonian fluid has an elastic component η'' that depends on the activity [11]. Simultaneous measurements of η'' and f_a shows that $\eta'' \propto f_a$. We quantify the activity with η'' because it has a significantly greater signal-to-noise ratio than $\langle \Delta r_1^2 \rangle$ and $\langle \Delta \alpha_1^2 \rangle$. Measurements of η'' average over the entire sample, or more than 10^5 particles, while measurements of $\langle \Delta r_1^2 \rangle$ and $\langle \Delta \alpha_1^2 \rangle$ average over the dyed particles in a frame, or about 10^2 particles.

Our results for different fiber concentrations are qualitatively similar, with strain thresholds roughly inversely proportional to the volume fraction. We present here the results of $c = 0.20$, which illustrate all the phenomena.

Upon commencement of oscillatory strain, the activity, as measured by η'', decays and vanishes in $\sim 10^2$ or fewer cycles for $\gamma < 2.2$, as shown in Fig. 2. For $\gamma > 2.8$, the activity initially decays but ultimately settles to a finite steady state value; the system remains irreversible. Between these values, the behavior is more complex, but an absorbing (reversible) state is eventually achieved where all activity ceases. For these larger strains, the orientation of the fibers evolves globally and gradually

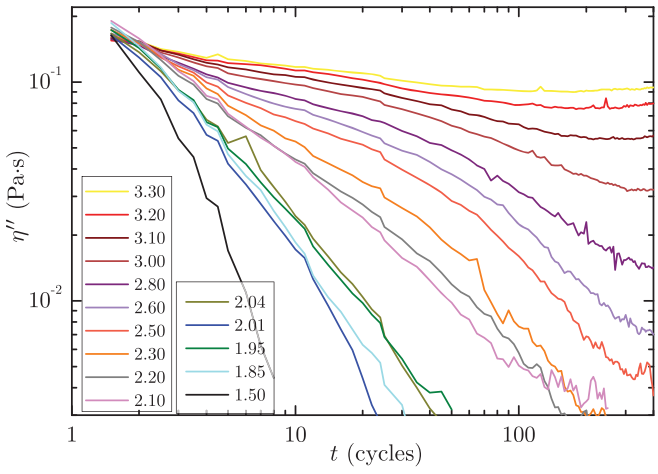

FIG. 2 (color). Rheological data showing decay of activity as measured by η'' for different strain amplitudes, as indicated in the legend.

with time such that the suspension ends in a nematic state, with the fibers aligned in the vorticity (z) direction. Images of the suspension, presented in Fig. 1, allow quantitative measurement of the distribution of angles α and ϕ, in the vertical (x-z) and horizontal (x-y) planes, respectively. We quantify the mean fiber orientation with two order parameters: $S_\alpha = 1 - 2\langle\cos^2\alpha\rangle$ and $S_\phi = 1 - 2\langle\cos^2\phi\rangle$. While nematic ordering is observed, as discussed below, there are no long range translational correlations.

We find that $S_\phi = -0.66 \pm 0.15$ remains constant independent of time and strain amplitude, which corresponds to fibers pointing on average about $24° \pm 6°$ from the flow direction, as observed in the x-y place. This result is near the -0.77 (or $20°$) value predicted by the Jeffery equations [21] corrected for elliptical particles [2].

The evolution of S_α is more complex. Figure 3 shows $S_\alpha(t)$ and the net change in orientation $\Delta S_\alpha = S_\alpha(\infty) - S_\alpha(0)$ of the steady state orientation relative to the initial orientation. The initial orientation $S_\alpha(0) = -0.21 \pm 0.04$ indicates that fibers are weakly oriented with the flow, consistent with the high strain protocol used before each measurement. At low strain amplitudes, there is no discernible change in the orientation. At moderate strain ($\gamma \approx 1.6$), ΔS_α increases as the activity persists for more than a few cycles. At higher strain ($2.6 \lesssim \gamma \lesssim 3$), the steady state orientation reaches a maximum ($S_\alpha(\infty) = 0.55 \pm 0.05$) as the suspension becomes nematic [Fig. 1(b)]. For strain amplitudes $\gamma \gtrsim 3$, ΔS_α decreases from this maximum value as the steady state fluctuations increase.

Rod orbits $\theta(\phi(t))$ are parameterized by two quantities, $\phi(0)$ (the initial azimuth) and $C \equiv \tan\theta(\phi = \pi/2)$ (the opening of the orbit) [21]. The distribution of ϕ does not change in time and thus is identical to the distribution of $\phi(0)$. The orbit parameter $C_b = C/(C+1)$ varies from 0 to 1 as the fiber tilts away from the vorticity (z) direction.

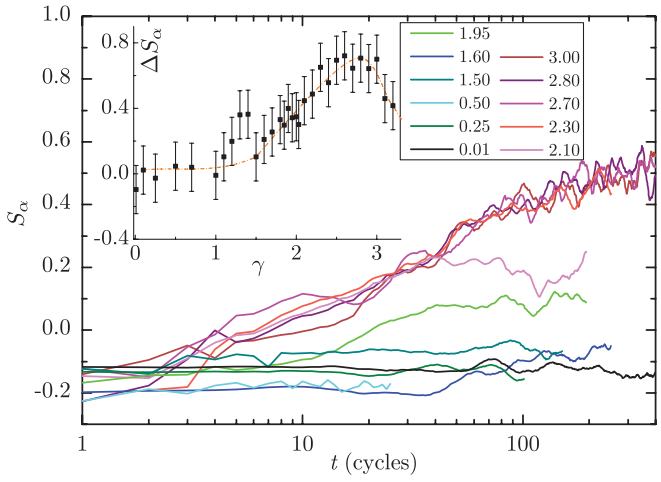

FIG. 3 (color). Temporal evolution of the average orientation in the x-z plane for different strain amplitudes, as indicated in the legend. Inset: Change in orientation $\Delta S_\alpha = S_\alpha(\infty) - S_\alpha(0)$.

When a fiber undergoes an irreversible displacement, C_b changes. Thus, activity can lead to a change in the distribution of C_b. Figure 4 shows distributions of C_b before and after runs at strains of 1.3 and 2.6. At low strains, the distribution of C_b remains rather flat with $\langle C_b\rangle \approx 0.3$, consistent with steady shear experiments [23]. At higher strains the distribution becomes strongly peaked around $C_b = 0.03$, as the fibers align with the vorticity. The peak is the highest for $\gamma = 2.6$, which corresponds to the greatest orientation with $\langle C_b\rangle \approx 0.094$.

The temporal evolution of fiber alignment affects how the system approaches the absorbing phase transition (APT), which is characterized by steady states that are either reversible ($\gamma < 2.7$) or irreversible ($\gamma \geq 2.7$). Fiber alignment is implicated because fibers aligned along the vorticity (z) direction are less likely to collide, thus promoting the reversible absorbing state.

Theories of APTs suggest that the activity η'' should scale [14,24], in analogy to equilibrium phase transitions, as

$$\eta''(\Phi, t) = \eta_0''|\Phi - \Phi_c|^\beta F(t/t_0|\Phi - \Phi_c|^\nu), \qquad (1)$$

where η_0'' and t_0 are the activity and cycle number at the start of the experiment, and β and ν are *rheological activity* and *time* scaling exponents, respectively. The control parameter Φ is defined in lattice models as the fraction of occupied sites. The value Φ_c separates absorbing states ($\Phi < \Phi_c$) from fluctuating states ($\Phi > \Phi_c$).

We make a connection with the theories of APTs by defining an effective volume fraction Φ of rods that governs whether or not fibers collide when the suspension is subjected to periodic shear. To determine Φ, we consider the mean-field volume $v(\gamma, C)$ swept out by a fiber during a

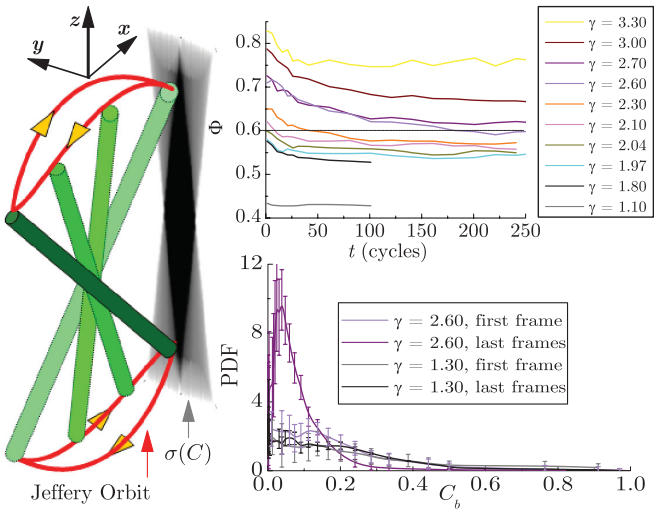

FIG. 4 (color). Left: Schematic of a Jeffery orbit and its projection (cross section) σ_C in shades of gray. Upper right: Temporal evolution of the control parameter Φ for different strains indicated in the legend. Dashed line indicates $\Phi_c = 0.60$. Lower right: Probability distribution function of $C_b = C/(C+1)$ for selected strains.

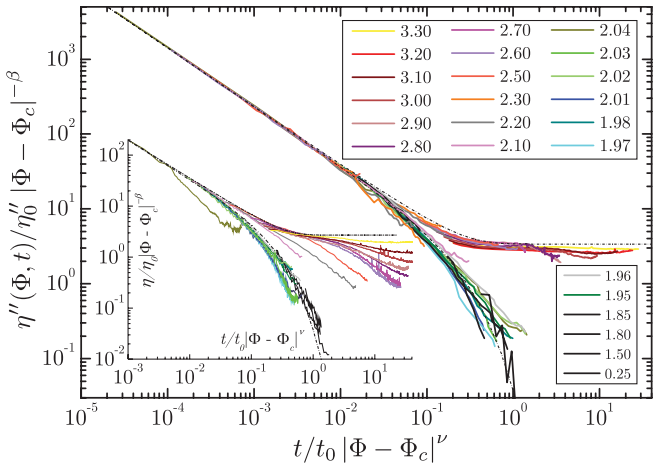

FIG. 5 (color). Rheological activity data rescaled using the scaling exponents $\beta = 0.86$ and $\nu = 1.09$, with strains indicated in the legend. Inset shows the best scaling that can be achieved when Φ is held constant, which is equivalent to using γ as the control parameter. The curve in the inset for $\gamma = 2.04$ starts on the critical line but falls off after about 6 cycles, consistent with the time at which $\Phi(t)$ falls below 0.6 (see Fig. 4 inset).

cycle, which depends on γ and C. For a strain amplitude γ, $v = v_f + v_C$, with v_f the fiber volume and v_C the mean volume swept out by the fiber cross-section σ_C averaged over a single-cycle and projected onto the gradient-vorticity plane (see Fig. 4). The effective fiber volume fraction is $\Phi(\gamma, t) = Nv(\gamma, t)/V$, with N the number of fibers and V the solution volume. Note that Φ decreases as fibers align with the vorticity, reflecting the reduced probability that oriented fibers have for colliding with one another. Figure 4 shows the temporal evolution of Φ at different strains and shows that Φ can decrease by 15% during an experiment.

To test the scaling hypothesis presented in Eq. (1), we plot $\eta''/\eta_0''|\Phi(t) - \Phi_c|^{-\beta}$ vs $t/t_0|\Phi(t) - \Phi_c|^{\nu}$, where η_0'' and t_0 are the activity and time, respectively, when the experiment starts, and where Φ_c, β, and ν are adjusted to achieve the best scaling. However, a curious problem arises when the data are scaled, as the data for $\gamma \lesssim 2$ scale best for choices of Φ_c near 0.6. The problem is that the scaling function F is expected to be different for $\Phi > \Phi_c$ and $\Phi < \Phi_c$; for several data sets, namely, those with γ near 2.1, the time-dependent effective volume fractions $\Phi(t)$ cross Φ_c (see Fig. 4). We deal with this issue by resetting t_0 and η_0'' to their values just after $\Phi(t)$ crosses Φ_c, consistent with the system starting anew with a different scaling function F. When this is done, we find that all the data, irrespective of whether or not $\Phi(t)$ crosses Φ_c, falls onto one of two scaling curves, one for $\Phi > \Phi_c$ and another for $\Phi < \Phi_c$. For $\Phi > \Phi_c$, the scaling function F goes to a finite value at large times, consistent with there being persistent activity above the transition. Conversely, for $\Phi < \Phi_c$, the scaling function F goes to zero at long times, consistent with activity disappearing at long times below the transition. This remarkable scaling is achieved for $\Phi_c = 0.60 \pm 0.01$, $\nu = 1.09 \pm 0.05$, and $\beta = 0.86 \pm 0.07$. The values of Φ_c, ν, and β, are consistent with the values 0.600, 1.081, and 0.827, respectively, expected for Manna universality class [11,14,25].

For comparison, the inset in Fig. 5 shows the best scaling that can be achieved if we assume that Φ remains constant in time. In this case, only the data for $\gamma \lesssim 2$ scales, which is consistent with our observation that the orientation of fibers is nearly constant over this range.

The ultimate temporal decay of the raw rheological data presented in Fig. 2 occurs with very nearly the same power law over a wide range of strain amplitudes, from $\gamma \approx 2.0$ to 2.7, suggesting a surprisingly wide range of critical or near critical behavior. This occurs because collisions between fibers cause the fiber orientation to continue to evolve as long as activity persists, which in turn increases the probability that the system will find an absorbing state. For sufficiently large γ, the alignment is no longer sufficient to permit the system to find an absorbing state. This picture is powerfully confirmed by the scaling of the activity presented in Fig. 5 together with the evolution of $\Phi(t)$ shown in Fig. 4.

We observe a striking shear-induced alignment of fibers with the vorticity direction. Mason [20] pointed out that a perfectly oriented suspension of non-Brownian rods is not stable under periodic drive, which would explain why the rods never achieve full alignment. More importantly, the alignment of fibers changes the probability of shear-induced collisions over time, which leads to a time-dependent control parameter. This can cause a system that is initially above Φ_c to fall below Φ_c. Surprisingly, the scaling behavior of the underlying absorbing phase transition is preserved, presumably because the time scale of the evolution of the orientation is slow compared to the activity relaxation time.

We thank P. Olmsted for helpful comments. This work was supported by the NSF through the NYU MRSEC, Award DMR:0820341. Additional support was provided by a Lavoisier Fellowship (A. F.) and from the Onassis Foundation (E. F.).

[1] C. A. Stover, D. L. Koch, and C. Cohen, J. Fluid Mech. **238**, 277 (1992).
[2] M. Rahnama, D. L. Koch, Y. Iso, and C. Cohen, Phys. Fluids A **5**, 849 (1993).
[3] M. Keshtkar, M. C. Heuzey, P. J. Carreau, M. Rajabian, and C. Dubois, J. Rheol. **54**, 197 (2010).
[4] M. Doi and S. F. Edwards, *The Theory of Polymer Dynamics* (Oxford University Press, Oxford, 1986).
[5] T. D. Papathanasiou, M. S. Ingber, and D. C. Guell, Compos. Sci. Technol. **54**, 1 (1995).
[6] O. D. Velev and S. Gupta, Adv. Mater. **21**, 1897 (2009).
[7] P. A. Lebwohl and G. Lasher, Phys. Rev. A **6**, 426 (1972).

[8] V. Narayan, S. Ramaswamy, and N. Menon, Science **317**, 105 (2007).
[9] V. Narayan and N. Menon, J. Stat. Mech. (2006) P01005.
[10] L. Onsager, Ann. N.Y. Acad. Sci. **51**, 627 (1949).
[11] L. Corté, P. M. Chaikin, J. P. Gollub, and D. J. Pine, Nature Phys. **4**, 420 (2008).
[12] D. J. Pine, J. P. Gollub, J. F. Brady, and A. M. Leshansky, Nature (London) **438**, 997 (2005).
[13] H. Hinrichsen, Adv. Phys. **49**, 815 (2000).
[14] S. Lubeck, Int. J. Mod. Phys. B **18**, 3977 (2004).
[15] M. Henkel, H. Hinrichsen, and S. Lubeck, *Nonequilibrium Phase Transitions: Absorbing Phase Transitions* (Springer, New York, 2008), p. 385.
[16] N. Mangan, C. Reichhardt, and C. J. Olson Reichhardt, Phys. Rev. Lett. **100**, 187002 (2008).
[17] C. Reichhardt and C. J. Olson Reichhardt, Phys. Rev. Lett. **103**, 168301 (2009).
[18] G. Krishnan, S. Beimfohr, and D. Leighton, J. Fluid Mech. **321**, 371 (1996).
[19] J. C. Crocker and D. G. Grier, J. Colloid Interface Sci. **179**, 298 (1996).
[20] A. Okagawa and S. G. Mason, Science **181**, 159 (1973).
[21] F. P. Bretherton, J. Fluid Mech. **14**, 284 (1962).
[22] L. Corté, S. J. Gerbode, W. Man, and D. J. Pine, Phys. Rev. Lett. **103**, 248301 (2009).
[23] M. Petrich, D. L. Koch, and C. Cohen, J. Non-Newtonian Fluid Mech. **95**, 101 (2000).
[24] K. A. Takeuchi, M. Kuroda, H. Chaté, and M. Sano, Phys. Rev. Lett. **99**, 234503 (2007).
[25] G. I. Menon and S. Ramaswamy, Phys. Rev. E **79**, 061108 (2009).